

Supporting Information

Bioinspired Compliance Grading Motif of Mortar in Nacreous Materials

Jabir Ubaid^a, Brian L. Wardle^b, and S. Kumar^{a,c,*}

^a Department of Mechanical Engineering, Khalifa University of Science and Technology, Masdar Campus, Masdar City, P.O. Box 54224, Abu Dhabi, UAE

^b Department of Aeronautics and Astronautics, Massachusetts Institute of Technology, Cambridge, MA 02139, USA

^c James Watt School of Engineering, University of Glasgow, Glasgow G12 8QQ, UK.
E-mail: s.kumar@eng.oxon.org

* Corresponding Author

S1. Geometric and material architecture of the nacreous structure.

The geometric configuration of experimentally realized nacreous structures (and subsequently also for the numerical analysis) is shown in Figure S1. The geometric and material properties of the nacreous structure are chosen such that the shear stress distribution in the mortar is quasi-uniform and the lowest feature size is an order of magnitude larger than the printer's resolution. E_b is the modulus of brick, E_m is modulus of homogeneous mortar, E_{mA} is modulus of region-A of tailored mortar and E_{mB} is modulus of region-B of tailored mortar. Nacreous structure consists of two brick-mortar layers of length, L_n and width, W_n and mortar layer of thickness t_{ml} between them.. The layers of the brick-mortar structure are at an offset in both x and y directions to each other. Together with the brick-mortar structure, grip spacers of length l_t and width W_n and thickness $2t + t_{ml}$ are printed using VeroWhite in order to clamp the samples during testing. Geometric details of a unit cell are given in Figure S1. Each of the bricks has length l_b , width w_b and thickness t . The mortar has a width w_m . Length of the tailored region-

B is denoted by l_B and the length l is defined such that $l_B/l = 1$, when region-B extends over the entire length of the horizontal mortar except for the region-A. Volume fractions of brick, mortar, region-A and Region-B in the experimentally realized nacreous systems are 69%, 31%, 2.2% and 5% respectively.

S2. Materials characterization

Mechanical properties of different 3D printed materials used in this study were evaluated through tensile tests performed on dogbone samples as per ASTM D412¹. Dogbone samples having gauge length of 25 mm, width of 6 mm and thickness of 2 mm were printed and tested. To perform digital image correlation (DIC) on the samples, random speckle patterns of white and black color were applied on the sample surfaces. First, white acrylic paint was sprayed on the sample surface using an air brush. After the white paint is completely dried, acrylic paint of black color was sprayed on the sample surface in random manner so as to get a random speckle pattern². Tensile tests of the dogbone samples were carried out using a Zwick-Roell universal testing machine. While the samples were loaded at a cross head speed of 5 mm/minute, images of the sample surfaces with the random speckle pattern were captured using CCD camera of 5.0 MP at 2 Hz using Vic-Snap software. Engineering stress, σ_{xx-eng} was calculated such that $\sigma_{xx-eng} = F/A_0$ where, A_0 is the original cross-sectional area and F is the load measured by the 2.5 kN load cell attached to the universal testing machine. Captured images were analyzed using Vic-2D software and point wise 2D surface engineering strains in the loading direction, transverse direction and the in-plane shear strain (ϵ_{xx-eng} , ϵ_{yy-eng} and ϵ_{xy-eng}) were computed. For the Young's modulus and Poisson's ratio calculations, average strain components for each image was computed by taking average of each strain component over an area in the gauge length of the samples. The edges of the sample were avoided in the strain calculation in order to avoid the errors associated inaccurate strains at the boundaries. Elastic moduli of three samples of each material were calculated by finding the initial slope of σ_{xx-eng}

– ε_{xx-eng} curves and Poisson’s ratio of each material were calculated by finding the initial slope of $\varepsilon_{yy-eng} - \varepsilon_{xx-eng}$ curves. Representative load-displacement curves of 3D printed materials used in this study are plotted in Figure S11 and their linear elastic properties are tabulated in Table S2.

S3. Effect of mortar stiffness on the mechanical performance of nacreous structures

Samples of non-tailored nacreous structures with different homogeneous mortar materials (Shore60 ($E_b/E_m = 834$), Shore50 ($E_b/E_m = 1468$), Shore40 ($E_b/E_m = 2044$) and TangoPlus ($E_b/E_m = 3309$); see Table S2) surrounding the bricks in all three directions were prepared utilizing multimaterial additive manufacturing. All the nacreous structures tested here have elastic non-dimensional number, $\beta_0 < 1$ ($\beta_0 = 0.079, 0.1001, 0.1187$ and 0.158 respectively) ensuring quasi-uniform shear stress distribution in the mortar. The aspect ratio of the bricks $\bar{b} = 10$ and the normalized overlap length between bricks $\bar{l} = 0.48$. An optical image of a 3D printed sample with the schematic of a unit cell indicating the horizontal and vertical mortars are shown in Figure S2. Mechanical tests were performed under monotonic tension. Figure S2 shows the load-displacement response of four different non-tailored nacreous structures together with the optical images captured when failure of the vertical mortar (corresponds to first peak in the load-displacement response) and when failure of the horizontal mortar (corresponds to second peak in the load-displacement response which also is the final failure of the structure) occur in each of the cases. It can be observed from Figure S2 that the load at which vertical mortar fails and that at which horizontal mortar fails increase with increase in elastic modulus of homogeneous mortar, leading to improved toughness of the nacreous system. During early stages of tensile loading, the vertical mortar takes more load relative to horizontal mortar and the tensile stress in the vertical bridges (mortar) further builds up with increase in load, eventually leading to failure of all vertically bridges at a load corresponding to first peak which is similar to observed behavior in natural nacre³⁻⁵.

Immediately after the first peak, there is a dip in the load-displacement response but the load transfer between bricks begins to wholly occur through the horizontal bridges, exhibiting work hardening response (albeit the slope of the curve is less than the initial slope) corresponding to resistance offered by the horizontal bridges due to frictional sliding. With further loading, the resistance increases to a maximum (corresponds to a global maximum in load-displacement curve) at which pull-out failure of bricks/platelets occur (see Figure S2). As discussed in the main text, mortar Shore50 (S50) was chosen for the baseline (see Figure 2 in the main text) because of the narrow window of material options available for multimaterial 3D printing.

References

- (1) Astm D412-16, Standard Test Methods for Vulcanized Rubber and Thermoplastic Elastomers—Tension. ASTM International: West Conshohocken, PA, 2016.
- (2) Cintron, R.; Saouma, V. Strain Measurements with the Digital Image Correlation System Vic-2d. *System* **2008**, *106*, 2D.
- (3) Slesarenko, V.; Kazarinov, N.; Rudykh, S. Distinct Failure Modes in Bio-Inspired 3d-Printed Staggered Composites under Non-Aligned Loadings. *Smart Mater. Struct.* **2017**, *26*, 035053.
- (4) Slesarenko, V.; Volokh, K. Y.; Aboudi, J.; Rudykh, S. Understanding the Strength of Bioinspired Soft Composites. *International Journal of Mechanical Sciences* **2017**, *131*, 171-178.
- (5) Kakisawa, H.; Sumitomo, T. The Toughening Mechanism of Nacre and Structural Materials Inspired by Nacre. *Science and Technology of Advanced Materials* **2012**, *12*, 064710.

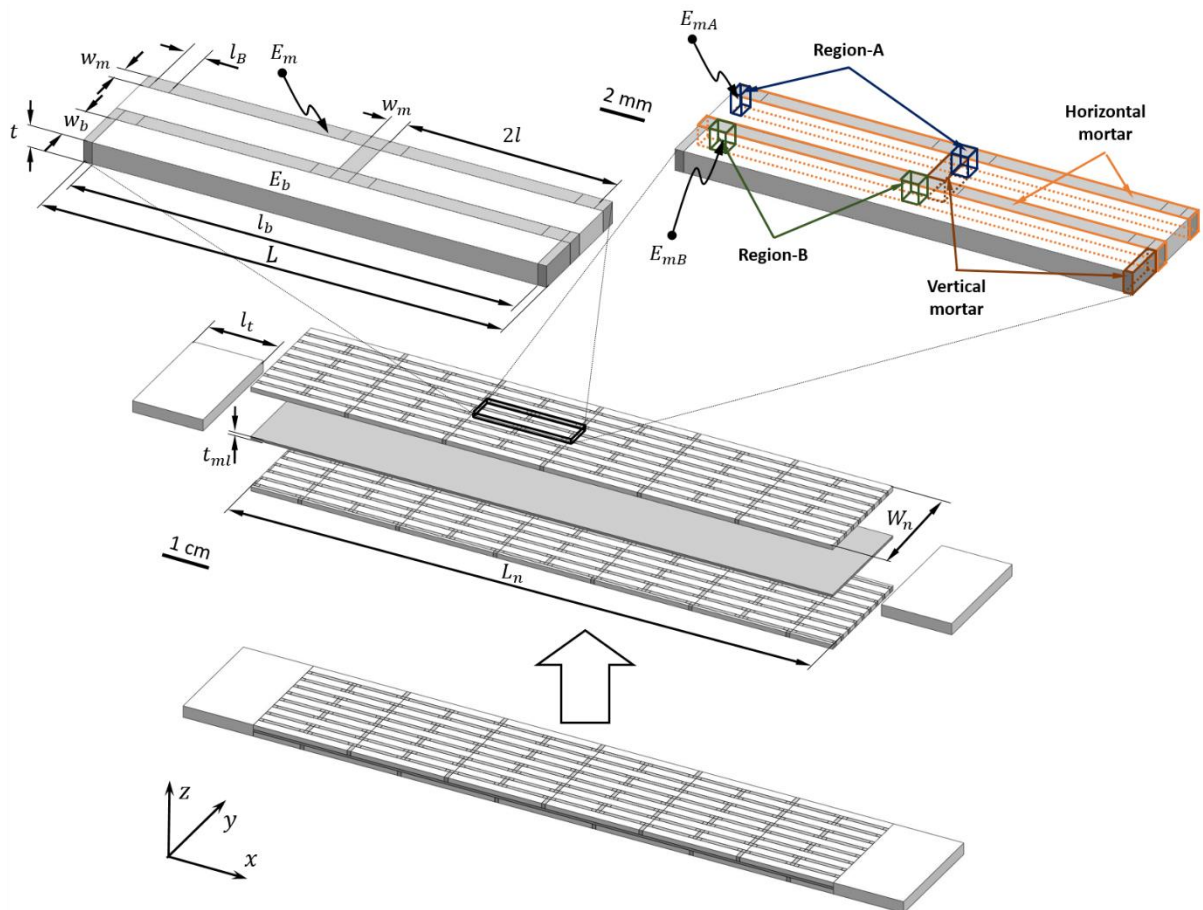


Figure S1. Geometric and dimensional configuration of one and two-layer nacreous structures. $l_b = 20$ mm, $w_b = 2$ mm, $t = 1$ mm, $w_m = 0.8$ mm, $l_B = 0.9$ mm, $2l = 9.6$ mm, $L = 20.8$ mm, $t_{mi} = 0.5$ mm, $L_n = 124$ mm, $W_n = 24.4$ mm and $l_t = 15$ mm.

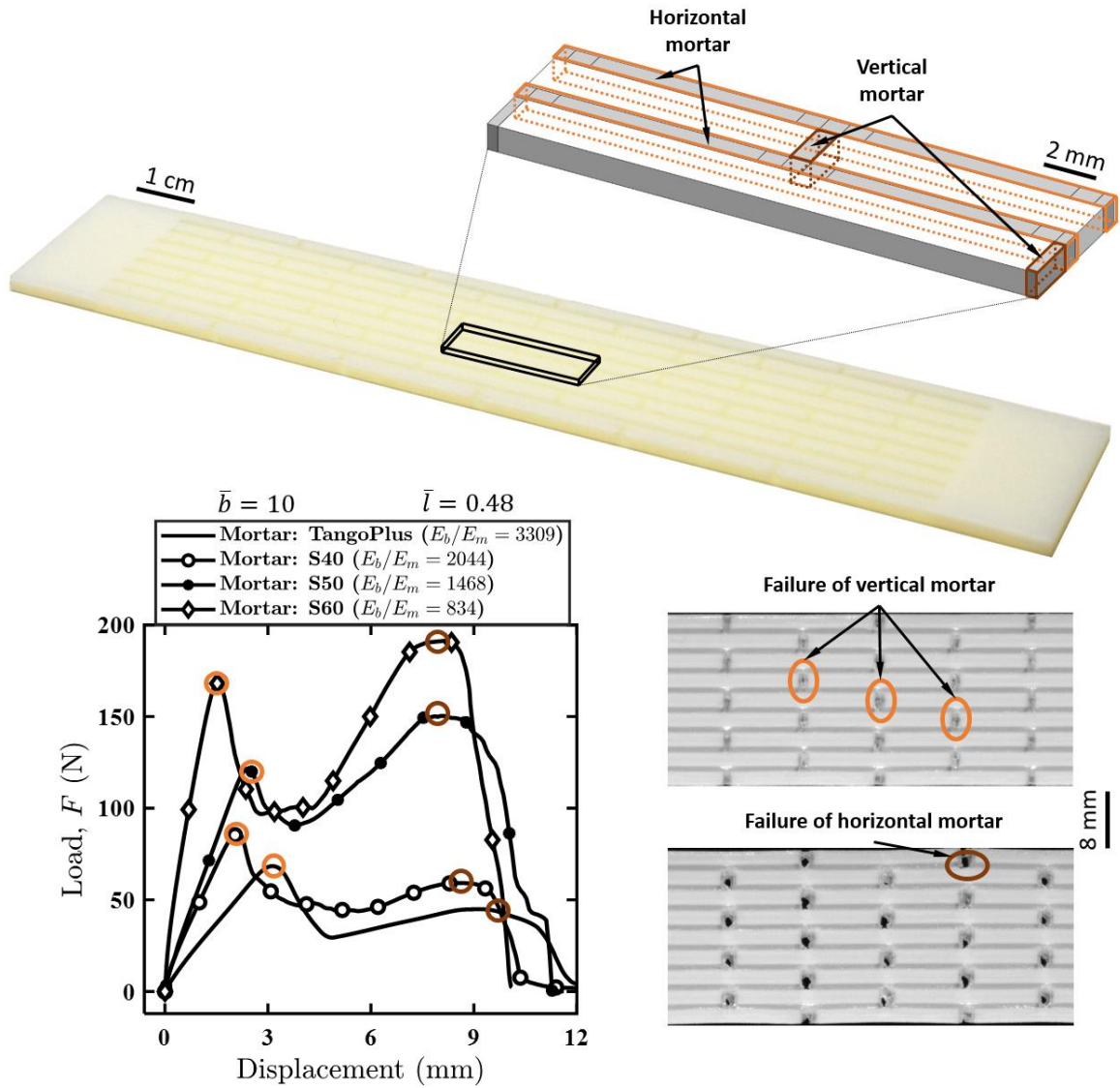


Figure S2. Experimental performance comparison of non-tailored nacreous structures with different mortar materials. Top image shows an additively manufactured nacreous structure sample with a schematic of unit cell where horizontal and vertical mortars are indicated. Bottom of the Figure shows load-displacement response of nacreous structures for four different choices of mortar together with optical images of the sample that indicates failure of vertical mortar and failure of horizontal mortar.

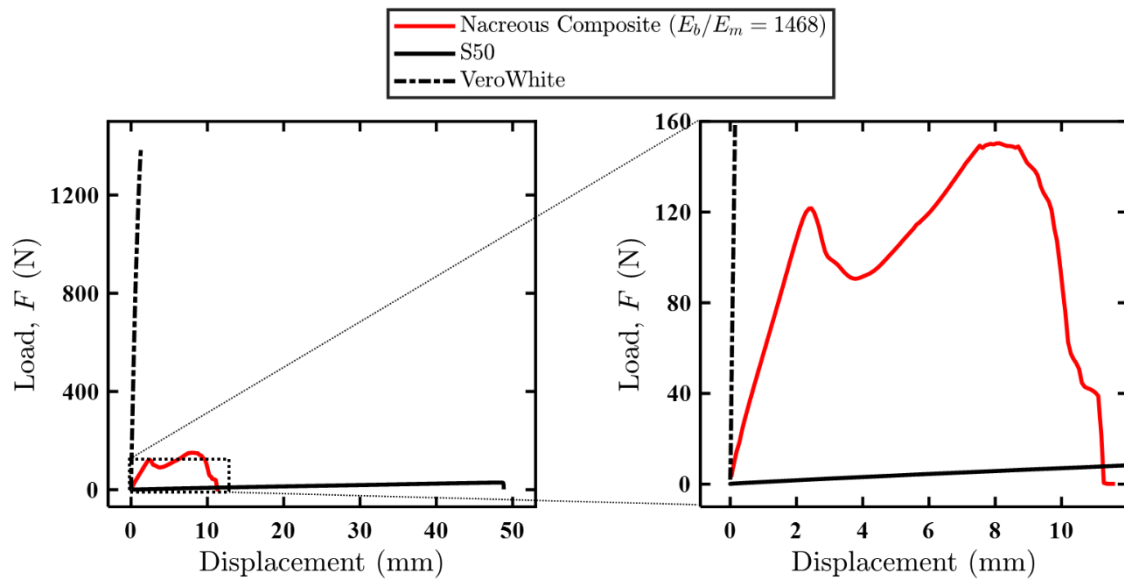


Figure S3. Experimental performance comparison of homogeneous plates of VeroWhite and S50 with nacreous structure of VeroWhite bricks and S50 mortar ($E_b/E_m = 1468$).

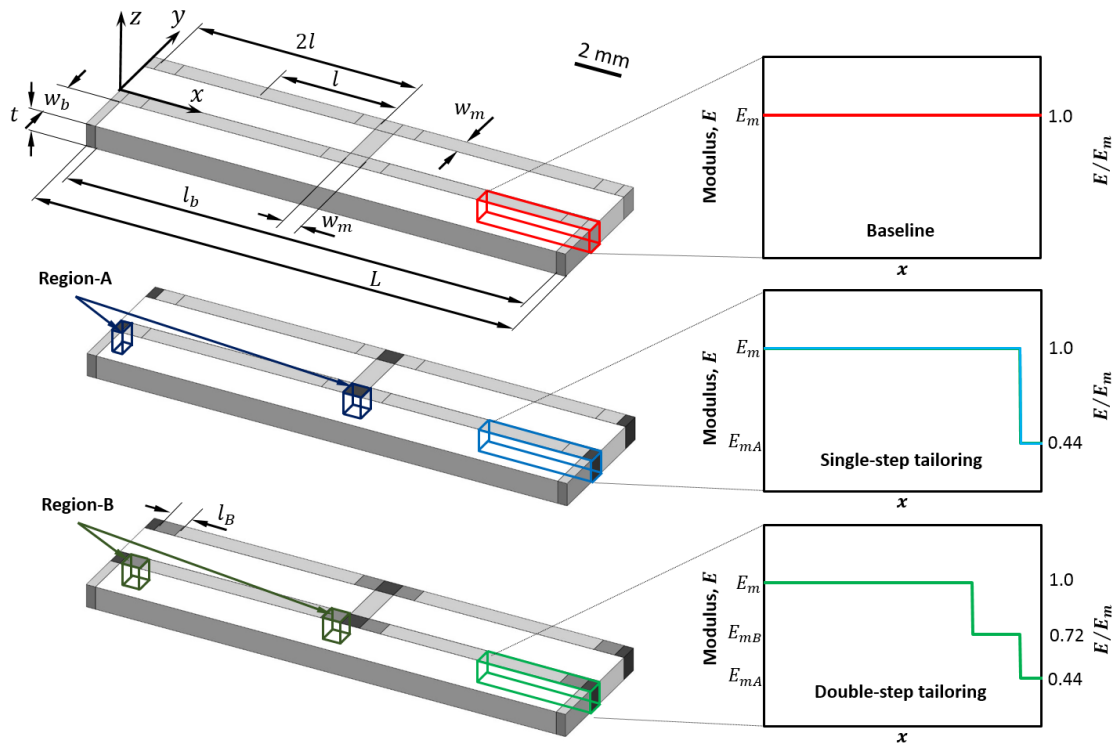


Figure S4. Schematic of unit cell of the baseline and tailored nacreous structures together with modulus variation of the mortar for two different schemes. In single-step tailoring scheme, the modulus varies from E_m (the baseline mortar modulus) to E_{mA} (the modulus in region-A of the mortar). In double-step tailoring scheme, the modulus varies from E_m to E_{mB} . E_{mB} is the modulus in region-B (of length l_b) of the mortar and $l_B/l = 0.1875$.

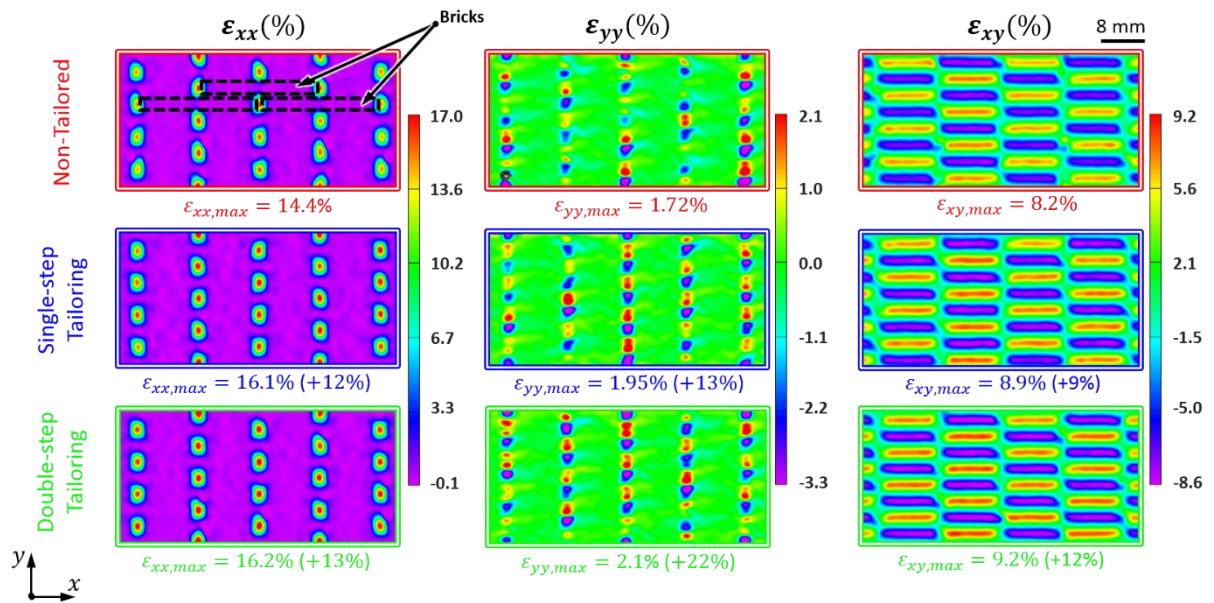


Figure S5. 2D full-field strain on the surface of the nacreous structures at a tensile load of 90 N (see Figure 2 in main text). ϵ_{xx} , ϵ_{yy} , and ϵ_{xy} indicate the longitudinal, peel and shear strains respectively. % changes given are from the baseline.

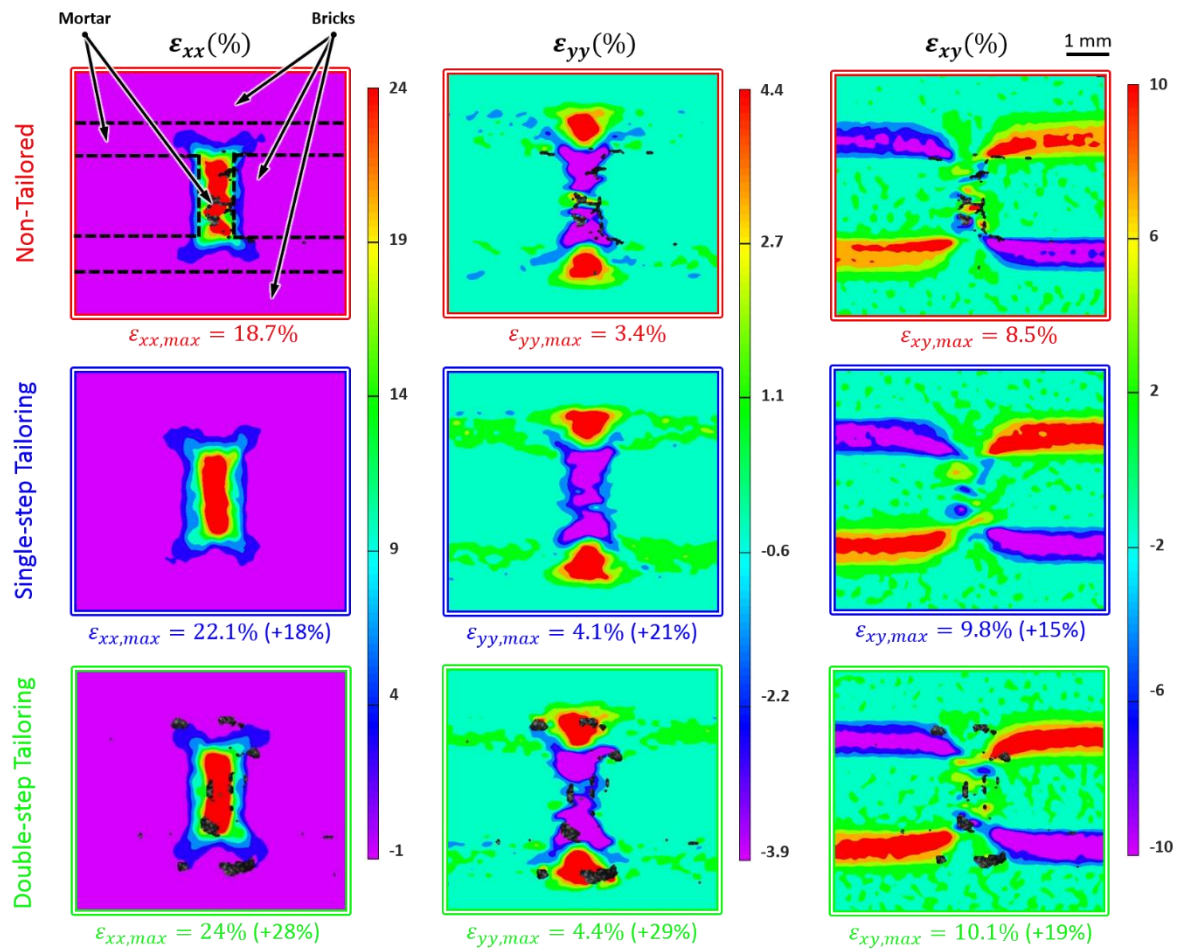


Figure S6. 2D full-field strain at a brick mortar intersection on the surface of the nacreous structures around a representative vertical mortar at a tensile load of 90 N (see Figure 2 in main text). ϵ_{xx} , ϵ_{yy} , and ϵ_{xy} indicate the longitudinal, peel and shear strains respectively. % changes given are from the baseline.

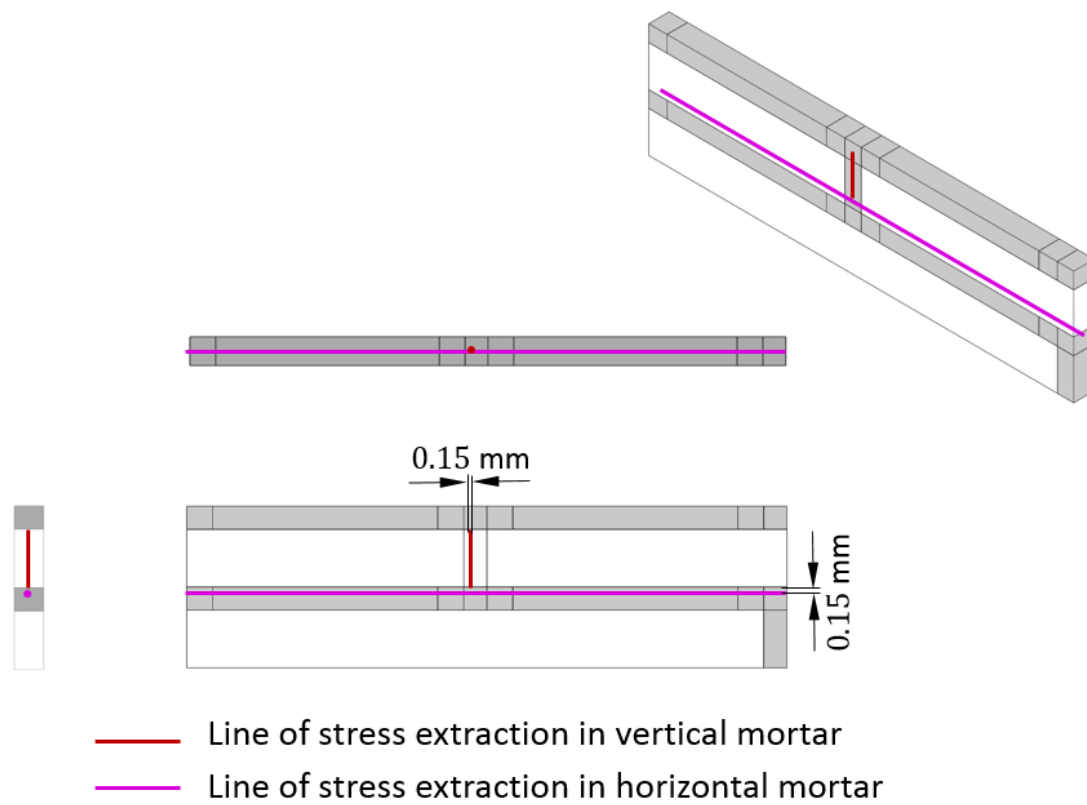


Figure S7. Schematic of a nacreous structure unit cell indicating lines in vertical and horizontal mortars through which the stresses are extracted in the FE study. Lines of stress extraction pass through layer midline and near the brick-mortar interface (0.15 mm from the interface).

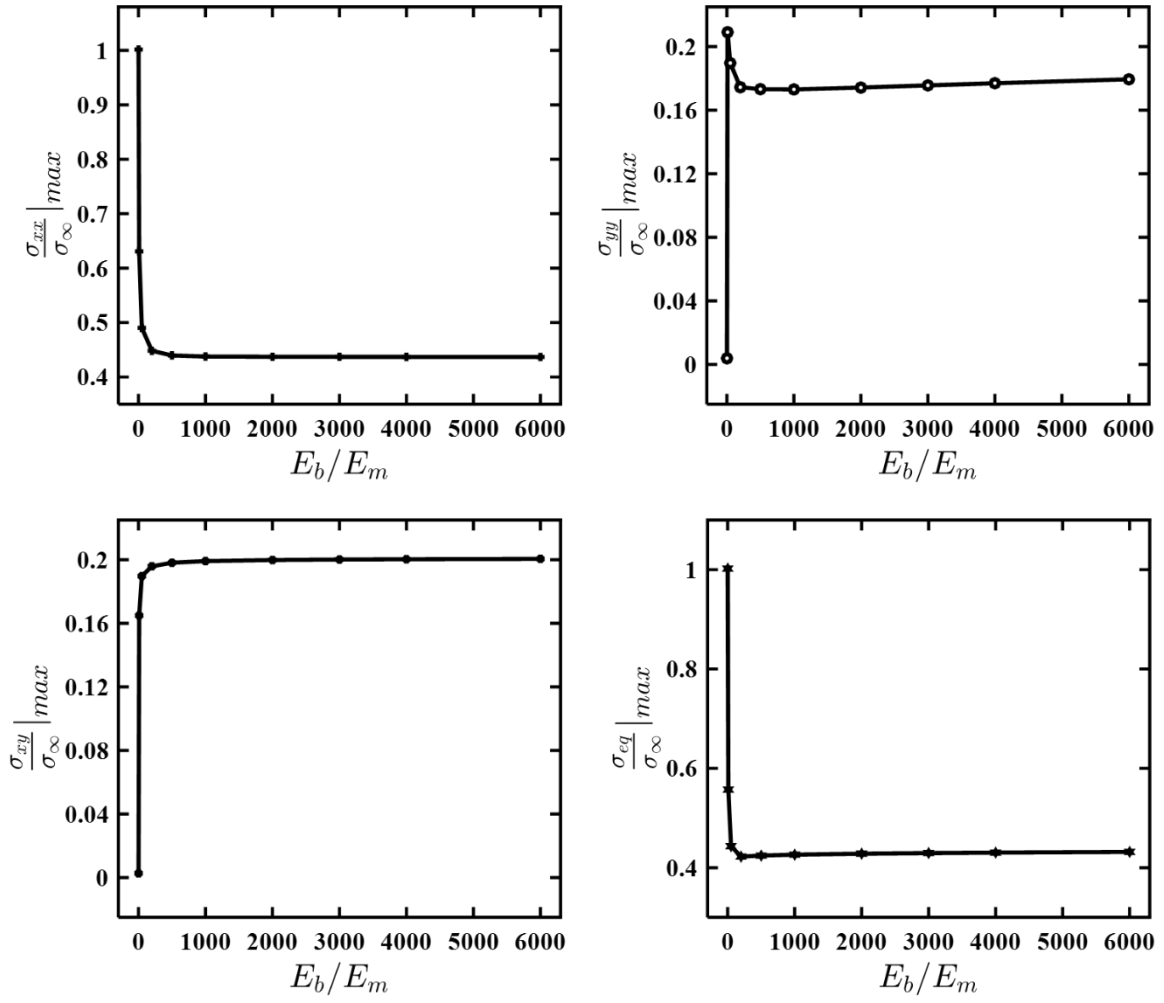


Figure S8. Maximum stress in the horizontal mortar from FE analyses: Maximum longitudinal, peel, shear and equivalent stresses in the horizontal mortar as a function of stiffness mismatch between bricks and mortar (E_b/E_m) for non-tailored nacreous structures. E_b is the modulus of brick and E_m is the modulus of baseline mortar. We take $\bar{b} = 10$ and $\bar{l} = 0.48$.

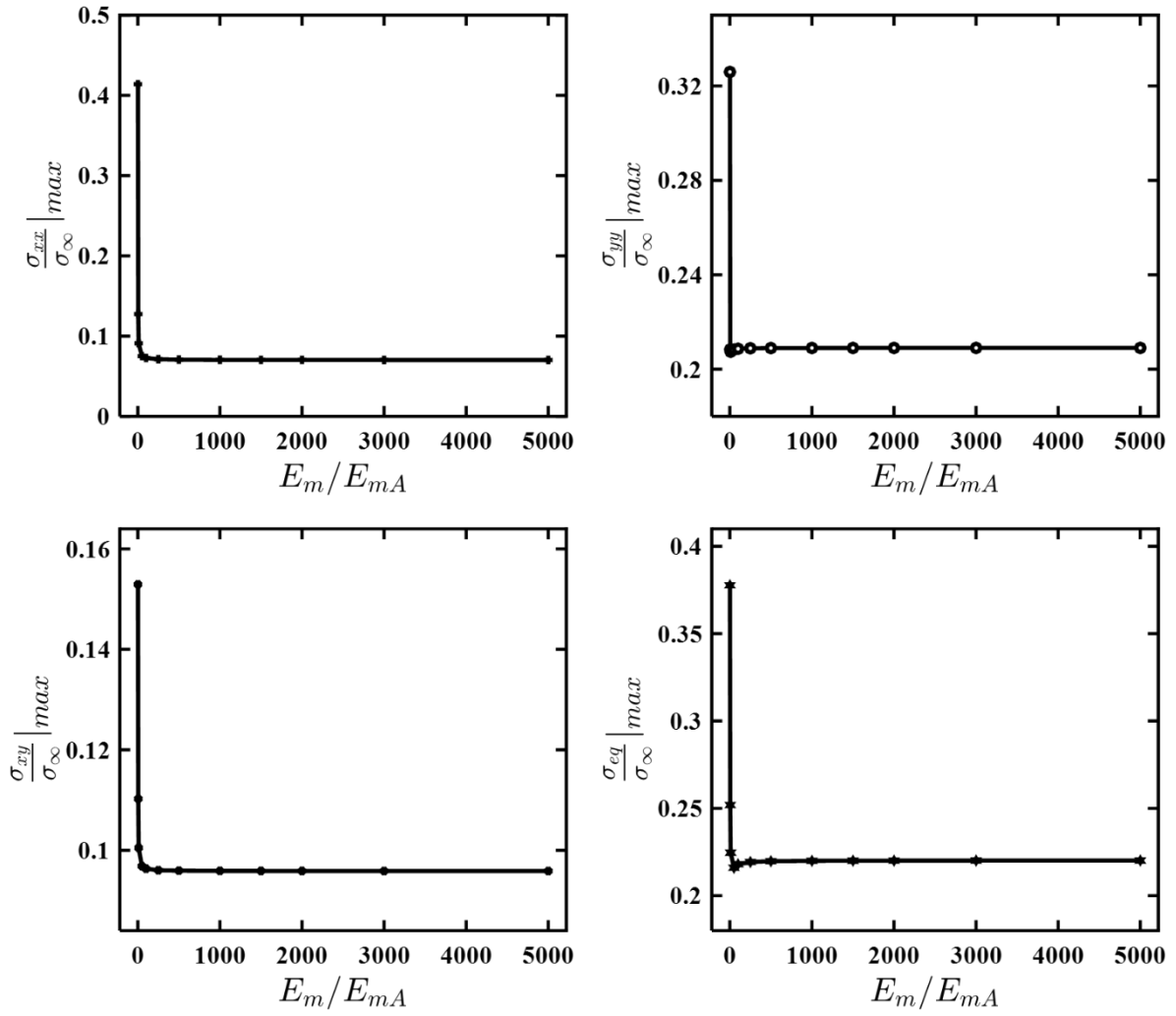


Figure S9. Maximum stress in the horizontal mortar from FE analyses: Maximum longitudinal, peel, shear and equivalent stresses as a function of modulus mismatch within the mortar (E_m/E_{mA}) for nacreous structures with single-step tailoring. E_{mA} is the modulus in region-A of the mortar. We take, $E_b/E_m = 500$, $\bar{b} = 10$ and $\bar{l} = 0.48$

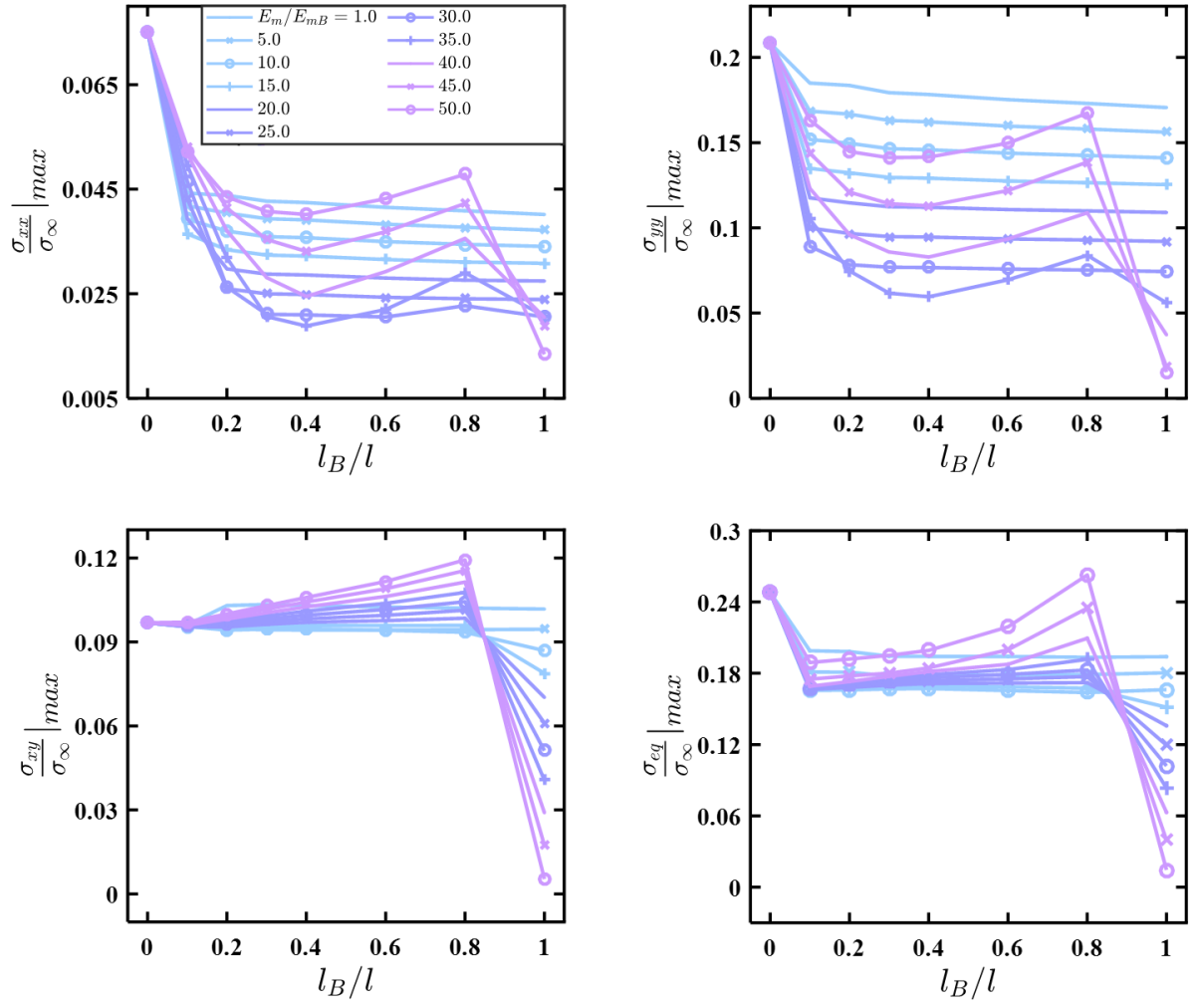


Figure S10. Maximum longitudinal, peel, shear and equivalent stresses in the horizontal mortar for different modulus ratios (E_m/E_{mB}) vs normalized length (l_B/l) for double-step tailored nacreous structures. E_m is the modulus of baseline mortar, E_{mB} is the modulus of region-B of mortar of length l_B . We take $E_b/E_m = 500$, $E_m/E_{mA} = 100$, $\bar{b} = 10$ and $\bar{l} = 0.48$

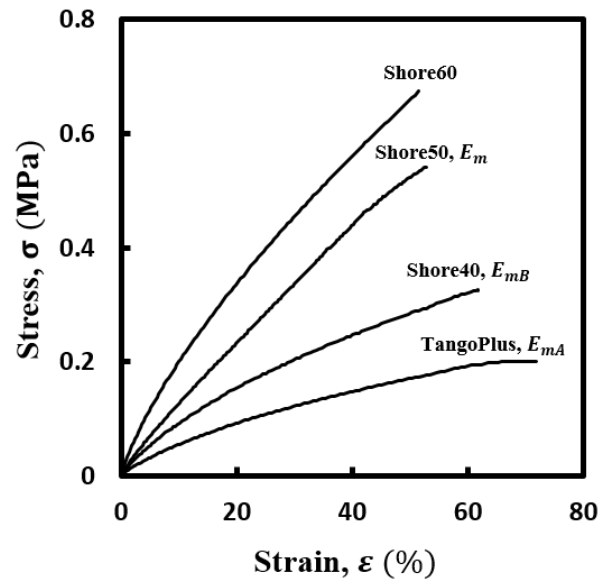
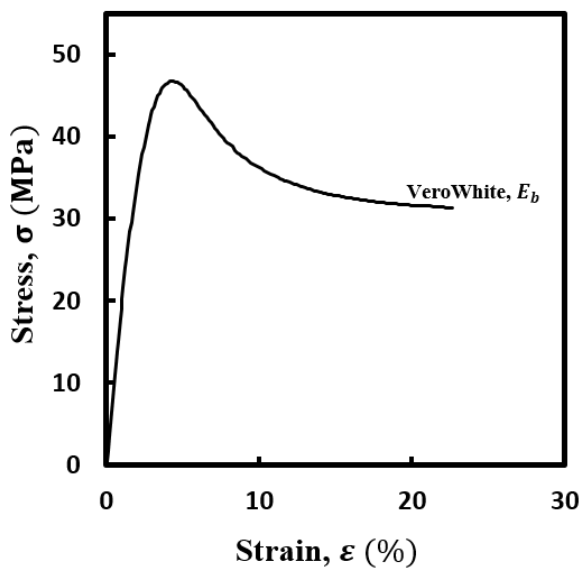


Figure S11. Representative load-displacement response of 3D printed materials used in this study for realizing various tailored nacreous structures.

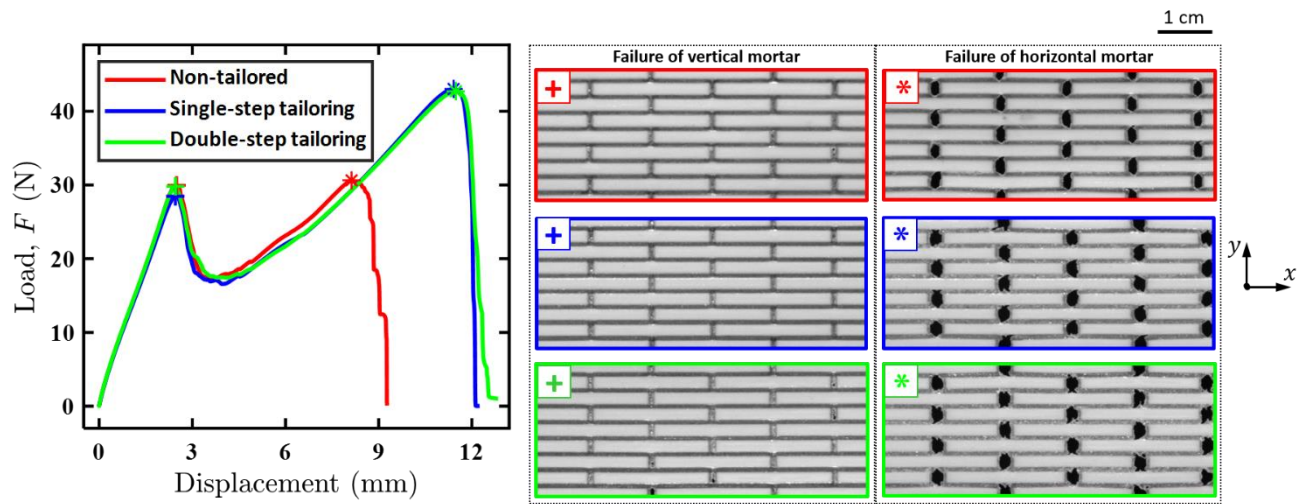


Figure S12. Representative load-displacement response together with optical images of the one-layer nacreous structure that indicate failure of vertical mortar (indicated by the first peak in the load-displacement response) and failure of horizontal mortar (ultimate failure, indicated by the second peak in the load-displacement response).

Table S1. Geometric parameters of nacreous structure

Length of brick, l_b	20 mm
Width of brick, w_b	2 mm
Thickness of brick mortar layer, t	1 mm
Width of mortar, w_m	0.8 mm
Length of region-B, l_B	0.9 mm
Overlap length, $2 * l$	9.6 mm
Length of unit cell, L	20.8 mm
Thickness of mortar between layers, t_{ml}	0.5 mm
Length of nacreous sample, L_n	124 mm
Width of nacreous sample, W_n	24.4 mm
Length of grip spacer, l_t	15 mm

Table S2. Linear elastic properties of 3D printed materials.

Material Name	Young's Modulus (MPa)	Poisson's Ratio
VeroWhite (E_b)	2,085	0.340
Shore60, S60	2.50	0.490
Shore50, S50 (E_m)	1.42	0.491
Shore40, S40 (E_{mB})	1.02	0.493
TangoPlus (E_{mA})	0.63	0.495

Table S3. Maximum longitudinal, peel and shear strains in the nacreous structures evaluated using digital image correlation (higher resolution). Significant changes from the baseline are indicated in red.

Design Configuration	Maximum longitudinal strain, ϵ_{xx} (%)	Maximum peel strain, ϵ_{yy} (%)	Maximum shear strain, ϵ_{xy} (%)
Baseline	18.7	3.4	8.5
Single-step tailoring	22.1 (+18%)	4.1 (+21%)	9.8 (+15%)
Double-step tailoring	24 (+28%)	4.4 (+29%)	10.1 (+19%)

Table S4. Summary of the experimental performance one-layer nacreous AM structures with standard error. Significant changes from the baseline (non-tailored) case are indicated in red.

Design Configuration	Initial stiffness (N/mm)	Load at first peak (N)	Maximum load (N)	Deflection at break (mm)	Modulus of toughness $\times 10^{-3}$ (Nm)
Baseline	14.01 \pm 0.21	29.9 \pm 0.17	30.6 \pm 0.72	8.1 \pm 0.15	195.5 \pm 2.7
Single-step tailoring	13.88 \pm 0.32	28.45 \pm 1.1 (-4.8%)	43.0 \pm 1.4 (+30.7%)	11.1 \pm 0.19 (+37.0%)	306.0 \pm 6.3 (+56.9%)
Double-step tailoring	13.83 \pm 0.47	29.5 \pm 1.3 (-1.3%)	42.3 \pm 1.8 (+38.3%)	11.2 \pm 0.5 (+38.3%)	312.5 \pm 8.5 (+60.3%)